Electronic structure, pressure- and temperature-dependent charge densities, and electric field gradients in FeF_2†

R. Reschke and A. Trautwein
Angewandte Physik, Universität des Saarlandes, 6600 Saarbrücken, West Germany

F. E. Harris
Department of Physics, University of Utah, Salt Lake City, Utah 84112
(Received 23 September 1976)

We derive the electronic structure of FeF_2 from molecular-orbital (MO) cluster calculations. FeF_2 is represented by a FeF_6^{4-} cluster. Pressure- and temperature-dependent cluster geometries are taken from the literature. The five configurations $^5B_{1g}$, $^5B_{2g}$, $^5B_{3g}$, ^5A_g, and $^5A'_g$, which we use to take into account configuration-interaction and spin-orbit coupling, are based on one-electron-MO functions. The energy separations of these configurations are scaled to match a particular experimental ΔE_Q value; reasonable agreement is thereby obtained over a range of temperature and pressure. The calculated pressure- and temperature-dependent electron charge densities and electric-field-gradient tensors at the iron nucleus are consistent with experimental isomer shifts, quadrupole splittings and asymmetry parameters in the paramagnetic phase as well as in the antiferromagnetic phase. Obtained energy separations are comparable with optical data.

I. INTRODUCTION

Ferrous fluoride (FeF_2) has been the subject of several studies dealing with Mössbauer spectroscopy; they report the temperature[1-7] and pressure dependences[8-13] of electric and magnetic hyperfine interactions. In addition, optical,[14,15] paramagnetic,[16,17] and antiferromagnetic[18] properties of the material have been investigated. The pressure-dependent isomer shift $\delta(p)$ of FeF_2 has been analyzed with the overlap distortion method[10] without simultaneously investigating the pressure and temperature dependence of the quadrupole splitting ΔE_Q. $\delta(T)$, on the other hand, was fitted with the Einstein formalism for the second-order Doppler shift and with an open parameter for the explicit temperature dependence of the isomer shift, however, without direct use of the electronic structure. The interpretation of the pressure-dependent quadrupole splitting[12,13] $\Delta E_Q(p)$ was based on a configuration-interaction formalism[19] neglecting, for example, Fe $4p$ and overlap contributions, and $\Delta E_Q(T)$ and $\delta(p, T)$ were not estimated simultaneously. $\Delta E_Q(T)$ has been analyzed on the basis of crystal-field theory (CFT).[2,4-7] Although on the CFT level of approximation, qualitatively correct results can be obtained especially for highly ionic compounds, anisotropic covalency effects Fe-$4p$ overlap, and lattice contributions are neglected, which have been shown to be of relative importance even in ionic compounds.[20-22] Moreover, pressure and (explicit) temperature dependences of electron densities at the iron nucleus cannot be described within the limitation of CFT.

We therefore found it worthwhile to derive the electronic structure of FeF_2 from molecular-orbital (MO) cluster calculations[23] which consistently describe pressure- and temperature-dependent isomer shifts and quadrupole splittings in the paramagnetic phase as well as in the antiferromagnetic phase.

II. STRUCTURAL DATA

FeF_2 has the rutile structure[17,24] belonging to the space group D_{4h}. Each ferrous high-spin iron is surrounded by a distorted octahedron of fluorine ions, and the point symmetry at the iron site is rhombic (D_{2h}). The cluster used in our MO calculations is FeF_6^{4-}. The iron-fluorine distances d_2 and d_4 in Fig. 1 and Table I and the angle which describes the rhombic distortion of the cluster are available from the literature for various pressures[11] (0, 58, 100, and 133 kbar at 300 K) and temperatures[25] (300, 400, 500, 600, 700 K at 0 kbar).

III. THEORETICAL BACKGROUND

The computational details of MO-cluster calculations,[23] of the evaluation of electric field gradients[22] V_{pq}, and of relativistic electron densities[26] $\rho(0)$, at the iron nucleus have been described elsewhere. Here we give some definitions which are used in the following.

Within the semiempirical MO-cluster approach, the empirical parameters for iron and fluorine are the same as previously used for iron-fluorine compounds.[23,27] With a Slater-type atomic-orbital (AO) basis set of Fe $3d$, $4s$, $4p$ and F $2s$, $2p$ orbi-

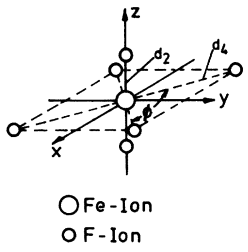

FIG. 1. FeF_6^{4-} cluster representing FeF_2 in MO cluster calculations. The crystallographic data are summarized in Table II.

TABLE I. Crystallographic data of FeF_2 (taken from Refs. 11 and 25).

		d_4 (Å)	d_2 (Å)	ϕ (deg)
p (kbar)	0	2.122	1.993	77.5
at 300 K	58	2.065	1.977	79.3
	100	2.035	1.969	80.3
	133	2.025	1.964	80.6
T(K)	400	2.123	1.996	77.6
at 0 kbar	500	2.124	2.000	77.7
	600	2.125	2.005	77.9
	700	2.126	2.010	78.1

tals we have for FeF_6^{4-} a total amount of 33 linear-combination-of-atomic-orbital MO's ϕ_i occupied by 54 valence electrons. The MO's $\phi_{25},\ldots,\phi_{29}$ are of mainly iron character [Fig. 2(a)]; their energy separations $\Delta_1,\ldots,\Delta_4$, depending on pressure and temperature, are drawn in Figs. 2(b) and 2(c), respectively. The corresponding changes of Fe 3d and Fe 4s occupancy with pressure and temperature are shown in Figs. 3(a) and (b), respectively. From the large isomer shift in FeF_2 (relative to metallic iron; see Fig. 17) it is obvious that the iron ion is in the ferrous high-spin state, hence, we construct configurations (Fig. 4) which are adequate to take into account configuration interaction[23] (CI) and spin-orbit coupling.[22]

An interesting feature of the limited CI calculation is represented by the following equations:

$$\begin{aligned}\Psi_1 &= 0.9998\,{}^5B_{1g} - 0.0013\,{}^5B_{2g} - 0.0209\,{}^5B_{3g},\\ \Psi_2 &= 0.0209\,{}^5B_{1g} + 0.1619\,{}^5B_{2g} + 0.9866\,{}^5B_{3g},\\ \Psi_3 &= -0.0021\,{}^5B_{1g} + 0.9868\,{}^5B_{2g} - 0.1619\,{}^5B_{3g}.\end{aligned} \quad (1)$$

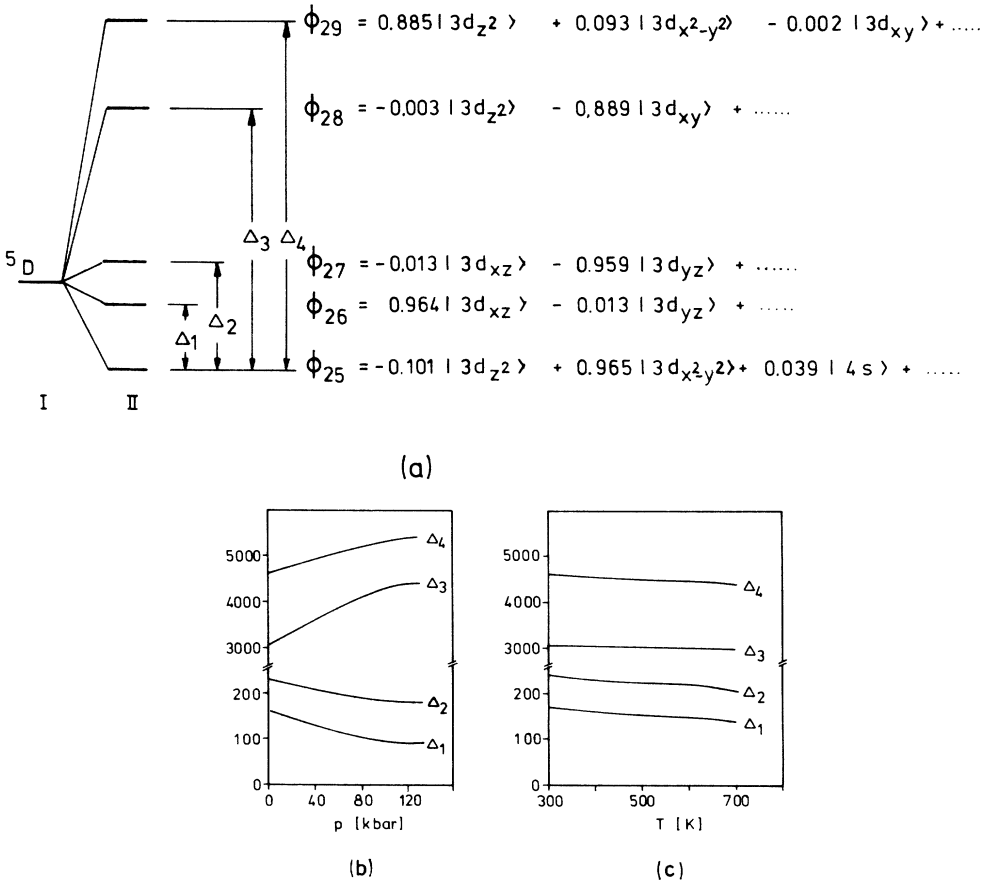

FIG. 2. (a) LCAO MO's ϕ_i and energy separations Δ_i in FeF_6^{4-} and their (b) pressure and (c) temperature dependence; calculated with the cluster geometries of Table I.

The energetically lowest CI state Ψ_1 is practically identical with configuration $^5B_{1g}$, the following CI state Ψ_2, however, consists mainly of configuration $^5B_{3g}$ with some contribution from configuration $^5B_{2g}$, the CI state Ψ_3 again is a mixture of configurations $^5B_{2g}$ and $^5B_{3g}$ with mainly $^5B_{2g}$ character. The sequence of Fe $3d$ orbitals which has been assumed in a ligand field study for the interpretation of $\Delta E_Q(T)$ of FeF_6 is qualitatively consistent with these CI results.

Spin-orbit coupling has been taken into account by first-order perturbation theory using in a first step as unperturbed states the five spin degenerated configurations of Fig. 4 and in a further step the CI states of Eq. (1).

Concerning V_{pq} we distinguish[22] valence contribution V_{pq}^{val} (Fe $3d$ and Fe $4p$ contribution), overlap contribution V_{pq}^{ov}, and lattice contribution V_{pq}^{lat}. In order to improve the estimate of V_{pq}^{ov} and V_{pq}^{lat} we—instead of Eqs. (18) and (20) in Ref. 22—use the approximation

$$V_{pq}^{ov+lat} = (1-\gamma_\infty)\sum_{A,B}\frac{3\bar{R}_p^{AB}\bar{R}_q^{AB}-\bar{R}_{AB}^2\delta_{pq}}{\bar{R}_{AB}^5}\,q_{AB}. \quad (2)$$

The summation is over all atoms A and B of the cluster. In case that $A \neq B$, then q_{AB} represents the overlap charge between atom A and atom B, and in case that $A = B$, then q_{AA} represents the charge of atom A. The charges q_{AB} are calculated from bond-order matrix elements $P_{\mu\nu}$ and overlap integrals $S_{\mu\nu}$:

$$q_{AB} = e\left(Z_A\delta_{AB} - \sum_{\mu,\nu} P_{\mu\nu}S_{\mu\nu}\right). \quad (3)$$

e is the positive elementary charge. The summation over μ includes atomic orbitals (AO) ψ_μ on center A, and that of ν includes AO's ψ_ν centered on atom B. The value eZ_A represents the core charge of atom A. The bond-order matrix elements are defined by

$$P_{\mu\nu} = \sum_{i=1}^{M} n_i c_{i\mu}c_{i\nu}. \quad (4)$$

M is the number of occupied MO's, $\phi_i = \sum_\mu c_{i\mu}\psi_\mu$, and $n_i = 1$ or 2 is the occupation number of MO ϕ_i. The Cartesian coordinates $\bar{R}_p^{AB}$ and the distance $\bar{R}_{AB}$ between iron and the various overlap charges q_{AB} are chosen as if the q_{AB} were situated at the maximum of product $\psi_\mu\psi_\nu$. Since the so defined overlap charges have a distance $\bar{R}_{AB}$ to iron larger than 1.6 Å in FeF_2, the use of $1-\gamma_\infty = 10.1$ is adequate.[28] This type of approximation for estimating V_{pq}^{ov+lat} takes better account of the charge distribution than the approximation described by Eqs. (18) and (20) of Ref. 12, which lumps together the whole charge distribution into point charges situated at the ligand sites. V_{zz}^{ov+lat} in FeF_2 is of the order -0.20 mm sec^{-1}, and in ferrocene[29] yields a value of even -0.9 mm sec^{-1}.

The total calculated charge density $\rho(0)$ consists of the valence contribution (Fe $4s$ and direct ligand-AO contribution at the iron nucleus) and of the core contribution

$$\rho(0) = \rho_{val}(0) + \rho_c(0). \quad (5)$$

$\rho_c(0)$ results from the iron core functions $\phi_{ns}(0)$, $(n = 1, 2, 3)$:

$$\rho_c(0) = 2\sum_{n=1}^{3}|\phi_{ns}(0)|^2, \quad (6)$$

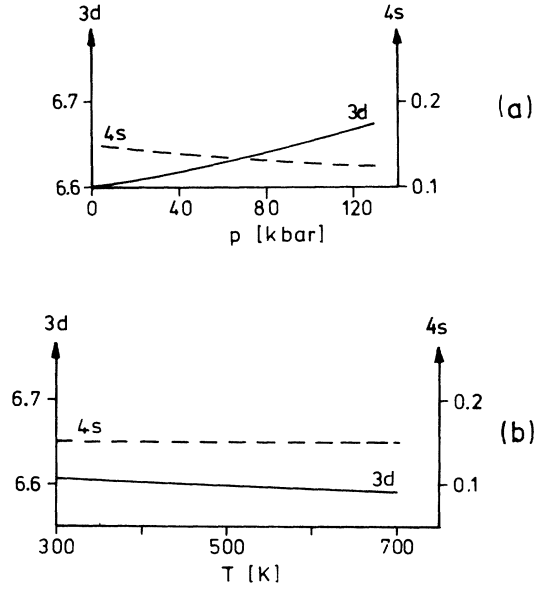

FIG. 3. Variation of Fe $3d$ and Fe $4s$ populations under the influence of (a) pressure- and (b) temperature-dependent cluster geometries.

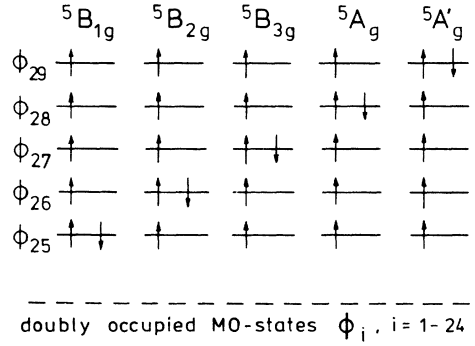

FIG. 4. Energetically low-lying $S = 2$ configurations with irreducible representations of the symmetry group D_{2h}.

TABLE II. Electric-field-gradient tensors V_{pq}, quadrupole splittings ΔE_Q, and asymmetry parameters η depending on the electronic structure of the FeF_6^{4-} cluster.

Configuration	V_{xx} [a]	V_{xy} [a]	V_{xz} [a]	V_{yy} [a]	V_{yz} [a]	V_{zz} [a]	ΔE_Q [a]	η
$^5B_{1g}$	−1.896	0.0	0.0	−1.537	0.0	3.432	3.439	0.105
$^5B_{2g}$	−1.237	0.0	0.0	3.205	0.0	−1.824	3.233	0.228
$^5B_{3g}$	4.101	0.0	0.0	−2.156	0.0	−1.945	4.103	0.051
^5A_g	−0.913	0.0	0.0	−1.896	0.0	2.809	2.866	0.350
$^5A_g'$	2.457	0.0	0.0	0.502	0.0	−2.959	−3.167	0.661
Ψ_1				same as $^5B_{1g}$				
Ψ_2	3.936	−0.867	0.0	−1.992	0.0	−1.944	4.059	0.042
Ψ_3	−1.074	0.867	0.0	3.041	0.0	−1.967	3.216	0.223

[a] Given in mm sec^{-1}.

where the ϕ_{ns} are orthogonalized to the M occupied cluster MO's ϕ_i. From known charge densities for various $3d^n 4s^m$ configurations[26] of the free-iron ion one may calculate by linear interpolation (this has been shown to be entirely satisfactory[26]) the charge density $\rho_p(0)$ the iron ion would have, if it were free but have the $3d^x 4s^y$ configuration which results from the MO-cluster calculations

$$\rho_p(0) = 2\sum_{n=1}^{3} |\psi_{ns}(0)|^2_{3d^x 4s^y} . \tag{7}$$

With the "potential contribution" $\rho_p(0)$ we define an "overlap contribution"

$$\rho_{ov}(0) = \rho_c(0) - \rho_p(0) . \tag{8}$$

IV. RESULTS AND DISCUSSION

A. Electric field gradient

1. Temperature dependence

Following the procedure described in Ref. 22 and in Sec. III we derive for the crystallographic structure of FeF_2 at 0 kbar and 300 K (see Fig. 1) electric-field-gradient tensors, quadrupole splittings (ΔE_Q), and asymmetry parameters (η) for the five configurations of Fig. 4 and for the three CI states of Eq. (1); these results are summarized in Table II. As a first rough estimate of the quadrupole splitting at 0 kbar and 300 K we neglect spin-orbit coupling, and we Boltzmann average the V_{pq} values of the five configurations in Table I using the energy separations Δ_i of Fig. 2. The calculated value of ΔE_Q^{calc} (0 kbar, 300 K) = 0.92 mm sec^{-1}, however, is far smaller than corresponding experimental values,[1,3,9] which are in the range 2.67 mm sec^{-1} $\leq \Delta E_Q^{expt}$ (0 kbar, 300 K) $\leq$ 2.79 mm sec^{-1}. This result is not surprising under the aspect that semiempirical MO calculations give energy separations which are usually reasonably relative values but not realistic absolute values. We therefore multiply our energies Δ_i with a factor f. The use of this factor does not change the electronic arrangement within the FeF_6^{4-} cluster since both secular problems

$$\det(\underline{F} - \epsilon \underline{S}) = 0 , \tag{9a}$$

$$\det(\underline{F}' - \epsilon' \underline{S}) = 0 \tag{9b}$$

result in identical MO's, if the Fock matrices $\underline{F}$ and $\underline{F}'$ are related by

$$\underline{F}' = f \underline{F} . \tag{9c}$$

Then the eigenvalues ϵ and ϵ' are related by

$$\epsilon' = f\epsilon . \tag{9d}$$

The influence of spin-orbit coupling (first-order perturbation) on ϵ' is shown in Fig. 5. The spin-orbit coupling constant in our calculation is −90 cm^{-3}. This value is smaller by 12% than the value −103 cm^{-1} for $3d^6$ configuration,[30] because of the reduced $\langle r^{-3} \rangle$ value for $3d^{6.6}$ configurations, which we find for FeF_2 from our calculations. We emphasize that covalency is automatically taken into account through the use of configurations as defined in Fig. 4. It is interesting to note that if

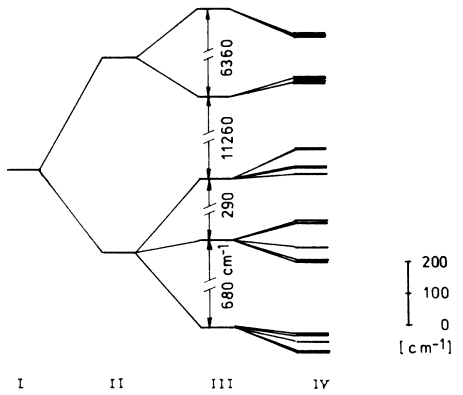

FIG. 5. Term splitting in FeF_2, calculated with crystallographic data for $p = 0$ kbar and $T = 300$ K (see Table I) and $f = 4$. I: free ion; II: O_h symmetry; III: D_{2h} symmetry; IV: D_{2h} symmetry and spin-orbit coupling.

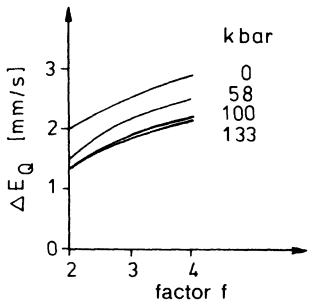

FIG. 6. Calculated quadrupole splitting at 300 K for various pressures and factors f (see text), taking account of spin-orbit coupling among the five configurations of Fig. 4 and the appropriate thermal populations of the 25 spin-orbit levels (see Fig. 5).

we had taken pure Fe $3d$ terms in our spin-orbit coupling scheme the covalent reduction would have led to the following effective spin-orbit coupling values (in cm^{-1}) for $3d^{6\cdot6}$ configuration

	ϕ_{25}	ϕ_{26}	ϕ_{27}	ϕ_{28}	ϕ_{29}
ϕ_{25}		−86	−85	−78	−78
ϕ_{26}			−85	−76	−76,
ϕ_{27}				−76	−76
ϕ_{28}					−72

which may be compared with the "isotropic" values $-69\ cm^{-3}$ (Ref. 2) and $-85\ cm^{-3}$ (Ref. 6) used in CFT calculations.

Taking into account spin-orbit coupling we finally get ΔE_Q values depending on the energy-scaling factor f (Figs. 6 and 7). The $\Delta E_Q(T)$ curves have been calculated with crystallographic data of FeF_2 for 0 kbar and 300 K; we therefore use these curves for the calibration of f by adjusting ΔE_Q^{calc} (0 kbar, 300 K) to ΔE_Q^{expt} (0 kbar, 300 K). With the resulting value $f = 3.7$ we then carry out all further calculations. In Table III, we compare our energy term scheme $\Delta E_i = 3.7\ \Delta_i$ with values from the literature.

So far, we did not take care of the changes in the geometry of the FeF_6^{4-} cluster with temperature. In Fig. 8, we show the influence of this temperature-dependent geometry effect upon $\Delta E_Q(T)$. Curve (a) is calculated with the five electronic configurations defined in Fig. 4, with energy separations ΔE_i of Table III, and taking account of spin-orbit coupling. Curve (b) is identical with curve (a) in the range $0 \leq T \leq 300$ K, however, at 400, 500, 600, and 700 K corresponding calculations have been performed with the relevant geometries defined in Table I, leading to temperature-dependent energy term schemes $\Delta E_i(T) = 3.7\ \Delta_i(T)$, with the $\Delta_i(T)$ values of Fig. 2(c). For comparison we give two additional curves. Curve (c) is calculated corresponding to curve (b) but with the configurations $^5B_{1g}$, $^5B_{2g}$, and $^5B_{3g}$ exchanged by the CI states Ψ_1, Ψ_2, and Ψ_3 defined in Eq. (1). This additional correction especially improves the low-temperature region of $\Delta E_Q(T)$; at temperatures $T > 300$ K curve (b) and (c) are practically identical. Curve (d) corresponds to $f = 2.8$, neglecting spin-orbit coupling but thermal averaging over the five configurations of Fig. 4. Although the geometrical temperature effect upon $\Delta E_Q(T)$ is much

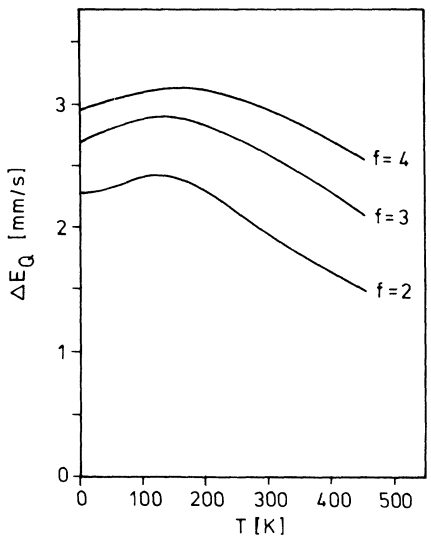

FIG. 7. $\Delta E_Q(T)$ curves depending on the energy scaling factor f, calculated with crystallographic data of FeF_2 for 0 kbar and 300 K.

TABLE III. Energy separations ΔE_i (cm^{-3}).

	Calculated values						
	This paper	Reference 2	Reference 5	Reference 6	Reference 7	Reference 13	Experimental values
ΔE_1	607	1000	821	780±40	767±53	760	
ΔE_2	873	2200	928	930±70	875±53	1060	1100[a]
ΔE_3	11 285		7642			4850	Approximately 9300[b]
ΔE_4	17 020		7642			6700	Approximately 11 150[b]

[a] J. W. Stout, M. I. Stienfield, and M. Yeezuri, J. Appl. Phys. 39, 1141 (1968).
[b] References 14 and 15.

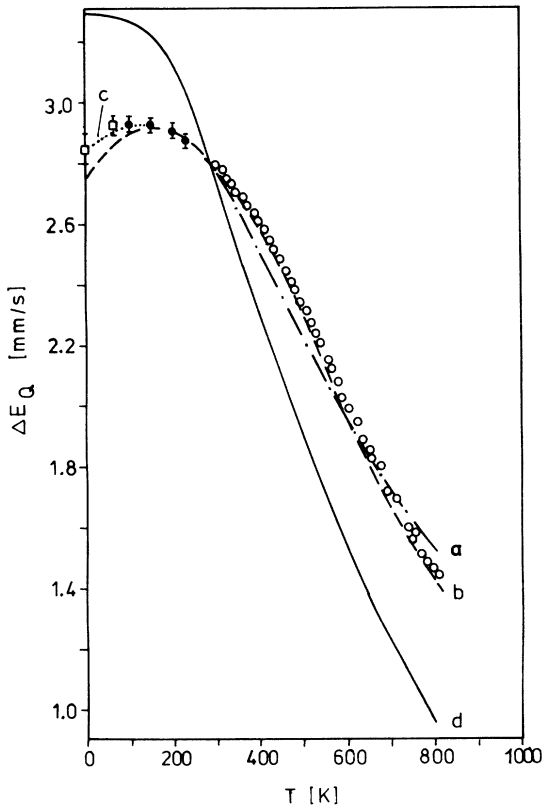

FIG. 8. Temperature-dependent quadrupole splitting of FeF_2, (a) calculated with the five configurations of Fig. 4, with energies ΔE_i of Table III ($f = 3.7$), and taking into account spin-oribt coupling (see text), (b) same as (a) but taking into account the thermal expansion of FeF_2, (c) same as (b) but with CI states instead of configurations, (d) $f = 2.8$, no spin-orbit coupling, but taking into account the simple thermal average over the five configurations of Fig. 4. Experimental values are taken from Refs. 1 and 3 (□), Ref. 6 (●), Ref. 7 (○), and Ref. 8 (△).

smaller than the effect, which is related to the thermal population of the 25 spin-orbit levels, it seems that the thermal expansion in FeF_2 detectably influences the quadrupole splitting above 300 K, it is, however, much better reflected in the temperature dependence of the asymmetry parameter η (Fig. 9). The orientation of the main component of the calculated V_{pq} tensor $V_{\bar{z}\bar{z}}$ remains along the z axis of Fig. 1 within the whole temperature range $0 \leq T \leq 800$ K. The only experimental information[3] concerning the orientation of $V_{\bar{z}\bar{z}}$ is that it is perpendicular to the crystallographic c axis ($\equiv y$ axis of Fig. 1), in agreement with our findings.

2. *Pressure dependence*

We now turn to the pressure-dependent quadrupole splitting of FeF_2 at 300 K. Experimental

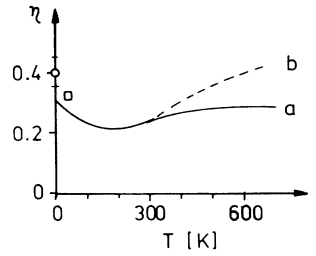

FIG. 9. Temperature-dependent asymmetry parameter of FeF_2, (a) and (b) correspond to curves (a) and (b) of Fig. 8, respectively. Experimental values are taken from Ref. 1 (□) and Ref. 3 (○).

$\Delta E_Q(p)$ values are available from Ref. 8. Using the pressure-dependent cluster geometries of Fig. 1, we calculate for pressures 0, 58, 100, and 133 kbar the electronic structure, and from this the quadrupole splitting at 300 K following exactly the procedure which led us to curve (b) of Fig. 8. In Fig. 10 we give experimental and theoretical $\Delta E_Q(p, 300\ \mathrm{K})$ results. It is worth noting that the energy-term scheme of Fig. 2(b), again using the scaling factor $f = 3.7$, leads to calculated $\Delta E_Q(p, 300\ \mathrm{K})$-values, which are in reasonable agreement with experiment. The asymmetry parameter increases considerably with increasing pressure (Fig. 11).

B. Magnetic properties

FeF_2 is antiferromagnetic[3] below $T_N = 78.2$ K. The exchange interaction of spins is described in the molecular field approximation[31] by an exchange field H_{exch}, in which the magnetic moments are aligned. Corresponding to our work on α-$FeSO_4$,[22]

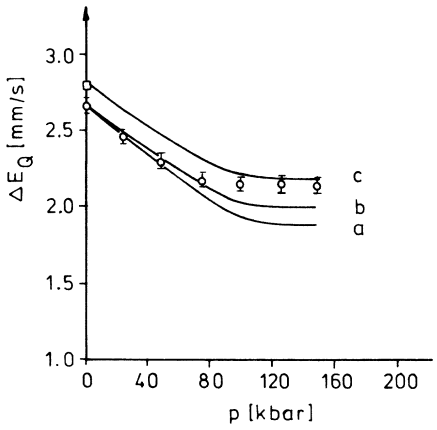

FIG. 10. Pressure-dependent quadrupole splitting of FeF_2, (a) calculated with $f = 2.6$ and neglecting spin-orbit coupling (b) $f = 3.3$ and taking into account spin-orbit coupling, (c) same as (b) but with $f = 3.7$ (experimental points taken from Ref. 8).

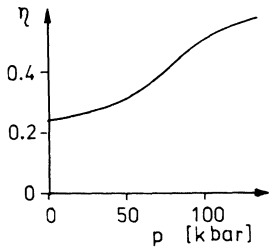

FIG. 11. Pressure-dependent asymmetry parameter of FeF_2.

we investigate for FeF_2 the influence of H_{exch} upon the spin orientation and the quadrupole splitting at temperatures $T < T_N$. On the basis of first-order perturbation calculations we study the influence of the exchange operator $\hat{H}_M = \mu_B(\hat{L} + 2\hat{S})\vec{H}_{exch}$ upon $|\alpha_j\rangle$ $(j = 1, \ldots, 25)$, which are eigenstates to the spin-orbit coupling operator $\hat{H}_{so} = \lambda\hat{L}\cdot\hat{S}$. With the spin being aligned along the crystallographic c $(\equiv z' \equiv y)$ axis[32] (in the saturated antiferromagnet) we can calculate $\langle S_{z'}\rangle_T$ depending on H_{exch} and T, as shown in Fig. 12. On the other hand, within the molecular field approximation, H_{exch} is proportional to the thermal average of the spin[31]:

$$H_{exch} = h\langle S_{z'}\rangle_T . \tag{10}$$

In order to derive $\langle S_{z'}\rangle_T$ values which are consistent with molecular-field theory for the whole antiferromagnetic range $T < T_N$, we draw the tangent to the $\langle S_{z'}\rangle_{78.2\,K}$ curve at 0 K (Fig. 12). The intersections of the straight line and the $\langle S_{z'}(H_{exch})\rangle_T$ curves yield the self-consistent values of $\langle S_{z'}\rangle_T$ for different temperatures T. For $T = 4.2$ K we obtain

$$\langle S_{z'}\rangle_{4.2\,K} = 1.98\,, \quad H_{exch} = 316 \text{ kOe}.$$

If we orient H_{exch} along the z axis of Fig. 1 (although it is known from experiment[32] that it is parallel to the crystallographic c axis; in our notation z', or y in Fig. 1) we derive the interesting result that $\langle S_z\rangle_{4.2\,K}$ is by far not saturated under an exchange field of about 320 kOe, whereas $\langle S_{z'}\rangle_{4.2\,K}$ is saturated already at about 50 kOe (Fig. 13). The ground state of the FeF_6^{4-} cluster is lowered by $H_{exch} = 330$ kOe, $\vec{H}_{exch} \| \vec{c}$ by 69.9 cm^{-1}, compared to 18.4 cm^{-1} if $\vec{H}_{exch} \perp \vec{c}$. The difference $\Delta = 69.9 - 18.4 = 51.5$ cm^{-1} is comparable with the anisotropy energy of 40 ± 2 cm^{-1} per ion found from antiferromagnetic-resonance measurements.[33]

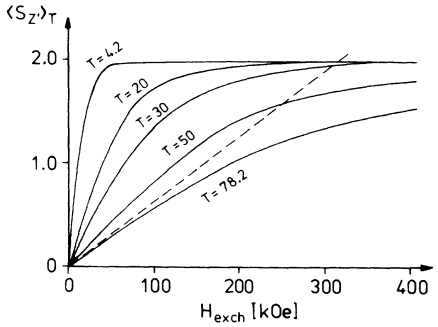

FIG. 12. Spin orientation along the crystallographic c $(\equiv z')$ axis in FeF_2 depending on exchange field $(\vec{H}_{exch} \| \vec{c})$ and temperature.

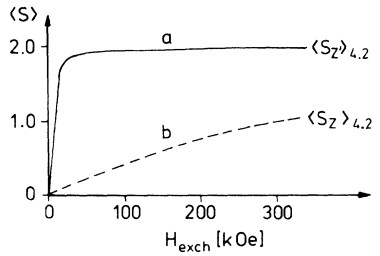

FIG. 13. Spin orientation at 4.2 K with $\vec{H}_{exch}$ (a) parallel to the crystallographic $\vec{c}$ axis and (b) perpendicular to $\vec{c}$, depending on the magnitude of $\vec{H}_{exch}$.

The presence of a magnetic field reorientates the spin-orbit states $|\alpha_j\rangle$ according to the interaction of the magnetic moment with $\vec{H}_{exch}$. Depending on the magnitude of $\vec{H}_{exch}$ we therefore may get appreciable mixing between the zero-field states $|\alpha_j\rangle$, and thus the quadrupole splitting might be different from that in zero field as was found for $\alpha - FeSO_4$ in the antiferromagnetic region.[22] Figure 14 shows the field dependence of $\Delta E_Q(T)$ from our calculations in which the electronic Hamiltonian contains also the interaction $\hat{H}_M$ with $\vec{H}_{exch} \| \vec{c}$. Consistent with the results in Fig. 8, curves (b) and (c) we find here that the magnetically induced quadrupole splitting in FeF_2 is practically negligible.

C. Charge densities

1. Pressure dependence

For the various structural geometries defined in Fig. 1 we calculate the charge density $\rho(0)$ and its contributions $\rho_{val}(0)$, $\rho_p(0)$, and $\rho_{ov}(0)$ along the lines described in Sec. III. Figure 15(a) shows the pressure dependence of these quantities. The decrease of $\rho_{val}(0)$ with increasing pressure is due

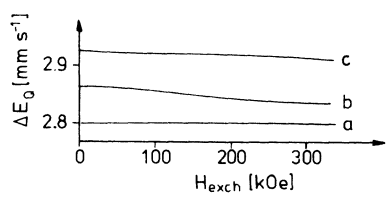

FIG. 14. Field dependence of ΔE_Q at temperatures (a) 4.2 K, (b) 40 K, and (c) 78.2 K.

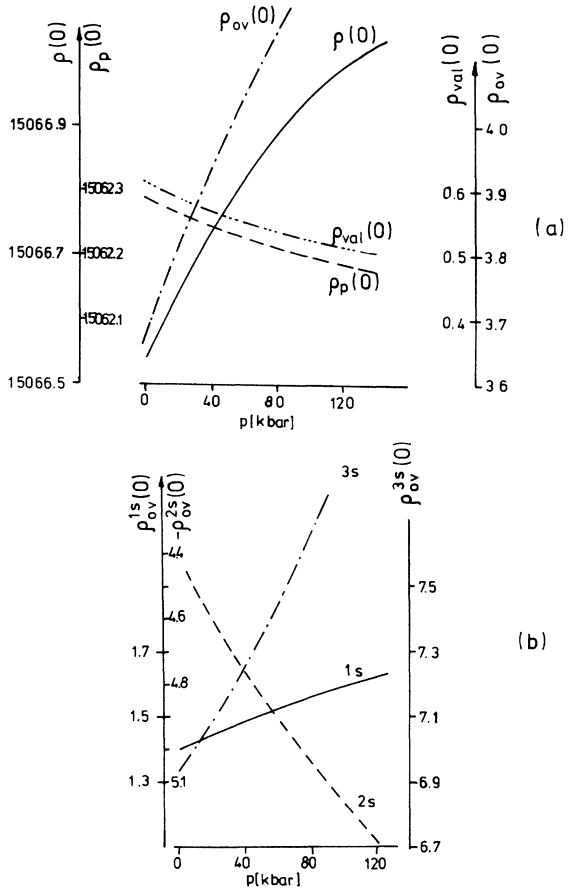

FIG. 15. Electron charge densities at the iron nucleus in FeF_2 depending on pressure. (a) $\rho(0)$ and contributions $\rho_{val}(0)$, $\rho_p(0)$, and $\rho_{ov}(0)$; (b) contributions from Fe 1*s*, 2*s*, and 3*s* electrons to $\rho_{ov}(0)$.

to the decrease of Fe 4*s* population [compare with Fig. 3(a)]; the corresponding decrease of $\rho_p(0)$ is due to the increase of Fe 3*d* population [compare also with Fig. 3(a)]. By far the largest contribution to the change of $\rho(0)$ with increasing p in FeF_2, however, comes from the overlap contribution $\rho_{ov}(0)$ due to the increased overlap between Fe-core *ns* orbitals and ligand-valence orbitals.[26,27] The different contributions from Fe 1*s*, Fe 2*s*, and Fe 3*s* electrons to $\rho_{ov}(0)$ are indicated in Fig. 15(b). It is characteristic for 2*s* electrons that $\partial\rho^{2s}_{ov}(0)/\partial p$ has the opposite sign compared with $\partial\rho^{1s}_{ov}(0)/\partial p$ and $\partial\rho^{3s}_{ov}(0)/\partial p$, because the orthogonalization terms in $\rho_{ov}(0)$ are sensitive[26] with respect to the Hartree-Fock functions at the iron nucleus, $\psi_{2s}(0)$ has opposite sign compared with $\psi_{1s}(0)$ and $\psi_{3s}(0)$.

Comparing our pressure dependent $\rho(0)$ values with experimentally determined pressure-dependent isomer shifts[8] δ we are able to derive the

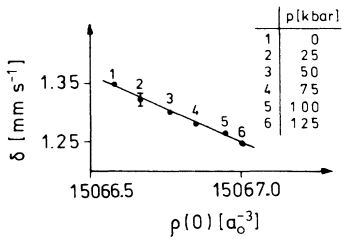

FIG. 16. Linear dependence between experimental pressure-dependent isomer shifts and calculated electron charge densities of FeF_2. Experimental isomer shifts at 300 K relative to metallic iron are taken from Ref. 8.

isomer-shift calibration constant α from

$$\Delta\delta = \alpha\Delta\rho(0). \tag{11}$$

From Fig. 16 we get $\alpha = -0.22 \pm 0.02 a_0^3$ mm sec^{-1}, in agreement with our previously obtained results for other compounds.[26,27,29]

2. *Temperature dependence*

The temperature dependence of the measured center shift comes from three different influences. (i) The implicit temperature dependence of the charge density is the product of two factors

$$\frac{\partial\delta^{\text{implicit}}}{\partial T} = \alpha\left(\frac{\partial\rho(0)}{\partial\ln(V/V_0)}\right)_T\left(\frac{\partial\ln(V/V_0)}{\partial T}\right)_p. \tag{12}$$

The term $(\partial\rho(0)/\partial\ln(V/V_0))_T$ describes the change of charge density with changing volume of the unit cell (T = const), and $(\partial\ln(V/V_0)/\partial T)_p$ stands for the change of volume with changing temperature (p = const). From our pressure-dependent charge densities and from the structural data of FeF_2—both summarized in Table IV—we derive

$$\frac{\partial\delta^{\text{implicit}}}{\partial T} = 0.997(\pm 0.091)\times 3.81\times 10^{-5}\ \text{mm sec}^{-1}\text{K}^{-1},$$

which is in reasonable agreement with experimen-

TABLE IV. Electron charge density at the iron nucleus (calculated for 0 (K) and volume of the unit cell of FeF_2 depending on various geometries.

Cluster geometry for p (kbar), T (K)	V (Å^3)	$\ln(V/V_0)$ [a]	$\rho(0)$ (a_0^{-3})
0, 300	73.003	0.0	15 066.579
0, 400	73.176	0.0024	15 066.571
0, 500	73.488	0.0066	15 066.551
0, 600	73.764	0.0104	15 066.525
0, 700	74.103	0.0150	15 066.523
58, 300	69.056	−0.0556	15 066.826
100, 300	66.957	−0.0864	15 066.968
133, 300	66.240	−0.0972	15 067.029

[a] V_0 is the volume of the unit cell at 0 kbar and 300 K.

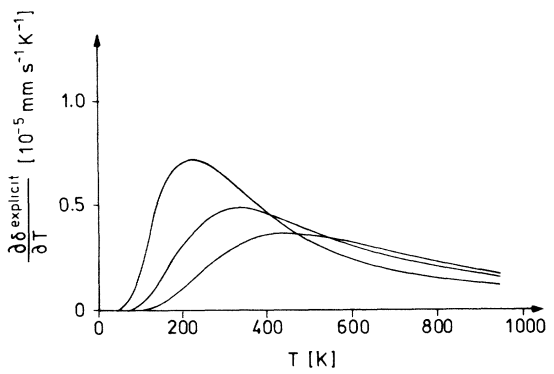

FIG. 17. Calculated explicit temperature dependence of the isomer shift.

tal results from Perkins *et al.*[7]:

$$\frac{\partial\delta^{implicit}}{\partial T} = 1.28\times 3.8\times 10^{-5}\ \text{mm sec}^{-1}\text{K}^{-1}.$$

(ii) The explicit temperature dependence of the charge density is due to thermal population of the 25 spin-orbit states $|\alpha_j\rangle$ having energies ΔE_j which might change Fe 4*s* and Fe 3*d* populations and hence $\rho_{val}(0)$ and $\rho_p(0)$:

$$\frac{\partial\delta^{explicit}}{\partial T} = \alpha\sum_{j=0}^{24}\rho(0_1\Delta E_j)\frac{\partial}{\partial T}[W(\Delta E_{j_1}T)]. \quad (13)$$

The probability function W describes the thermal population of state $|\alpha_j\rangle$, and $\partial W/\partial T$ is given by

$$\frac{\partial W(\Delta E_{j_1}T)}{\partial T} = \frac{W(\Delta E_{j_1}T)}{f_2T^2} \times\sum_{i=0}^{24}[\Delta E_j\delta_{ij} - W(\Delta E_{i_1}T)\Delta E_i]. \quad (14)$$

Figure 17 shows $\partial\delta^{explicit}/\partial T$ depending on T and on the energy scaling factor f described in Sec. IV A. It is obvious that $\partial\delta^{explicit}/\partial T$ is not constant, as sometimes assumed in the literature [see below under (iii)]. We do not consider, however, our results in Fig. 17 to be quantitative, since the changes in Fe 3*d* population associated with $\partial\delta^{explicit}/\partial T$ over the whole temperature range of $0<T<800$ K are only of the order 0.5% of the total Fe 3*d* population. (iii) The second-order Doppler shift δ_{SD} contributes more to the temperature dependence of the center shift than the other two contributions described above. Within the Debye approximation δ_{SD} is given by[34]

$$\delta_{SD}(T) = -2.7\times 10^{-4}\Theta_D - 7.2\times 10^{-4}Tf(T/\Theta_D), \quad (15)$$

with $f(T/\Theta_D)$ being the Debye function.[31,34] Under the approximation that the explicit temperature dependence $\partial\delta^{explicit}/\partial T$ is a constant, the total center shift can be written in the following way[7]:

$$\delta(T) = \delta_0 + \left(\frac{\partial\delta^{implicit}}{\partial T} + \frac{\partial\delta^{explicit}}{\partial T}\right)T + \delta_{SD}(T). \quad (16)$$

The constant δ_0 represents the isomer shift of FeF_2 at 0 K with respect to α-Fe metal at 300 K. Using the experimental center shift values of Johnson *et al.*[6] for $T<300$ K and of Perkins *et al.*[7] for $T>300$ K we get for the three fit parameters δ_0, $\partial\delta^{explicit}/\partial T$, and Θ_D of Eq. (16), taking the value $\partial\delta^{implicit}/\partial T$ from (i), the values

$$561\ \text{K} \leq \Theta_D \leq 484\ \text{K},$$

$$1.621\ \text{mm sec}^{-1} \leq \delta_0 \leq 1.603\ \text{mm sec}^{-1},$$

$$-7.25\times 10^{-5}\ \text{mm sec}^{-1}\text{K}^{-1} \leq \frac{\partial\delta^{expl}}{\partial T} \leq -6.61\times 10^{-5}\ \text{mm sec}^{-1}\text{K}^{-1}.$$

The values of Perkins *et al.*,[7] which have been obtained on the basis of the Einstein model for δ_{SD} and using experimental values in the range 300 K $<T<$ 965 K,

$$\Theta_E = 350\ \text{K (corresponds to } \Theta_D \sim \tfrac{3}{2}\Theta_E),$$

$$\delta_0 = 1.599\ \text{mm sec}^{-1},$$

$$\frac{\partial\delta^{explicit}}{\partial T} = -(6\pm 1)\times 10^{-5}\ \text{mm sec}^{-1}\text{K}^{-1},$$

agree reasonably well with our values above. At this point we want to emphasize again that the analysis of experimental $\delta(T)$ data along Eq. (16), and especially the derived value of $\partial\delta^{explicit}/\partial T$ is at most of qualitative value, since we have shown under (ii) that this value must not be a constant.

V. CONCLUSION

On the basis of semiempirical MO-cluster calculations with a FeF_6^{4-} cluster representing FeF_2 and with configuration interaction and spin-orbit coupling being taken care of, we derive the temperature- and pressure-dependent electronic structure of ferrous iron fluoride. We find that the derived energies are comparable with optical data and that the calculated pressure- and temperature-dependent electron-charge densities and electric-field-gradient tensors at the iron nucleus are consistent with experimental isomer shifts, quadrupole splittings, and asymmetry parameters in the paramagnetic phase as well as in the antiferromagnetic phase.

†Supported in part by Deutsche Forschungsgemeinschaft and in part by an award from the Biomedical Sciences Support Grant at the University of Utah.

[1]C. K. Wertheim, Phys. Rev. 121, 63 (1961).
[2]R. Ingalls, Phys. Rev. 133, A787 (1964).
[3]C. K. Wertheim and D. N. E. Buchanan, Phys. Rev. 161, 478 (1967).
[4]R. C. Axtmann, Y. Hazony, and J. W. Hurley, Jr., Chem. Phys. Lett. 2, 673 (1968).
[5]U. Ganiel and S. Shtrikman, Phys. Rev. 177, 503 (1969).
[6]D. P. Johnson and R. Ingalls, Phys. Rev. B 1, 1013 (1970).
[7]H. K. Perkins and Y. Hazony, Phys. Rev. B 5, 7 (1972).
[8]A. R. Champion, R. W. Vaughan, and H. G. Drickamer, J. Chem. Phys. 47, 2583 (1967).
[9]E. Šimánek and A. Y. C. Wong, Phys. Rev. 166, 348 (1968).
[10]H. G. Drickamer, S. C. Fung, and G. K. Lewis, Jr., in *Advances in High Pressure Research* (Academic, New York, 1969), Vol. 3.
[11]C. W. Christoe and H. G. Drickamer, Phys. Rev. B 1, 1813 (1970).
[12]D. M. Silva and R. Ingalls, Phys. Rev. B 5, 3725 (1972).
[13]D. M. Silva, Phys. Rev. B 7, 3306 (1973).
[14]G. D. Jones, Phys. Rev. 155, 259 (1967).
[15]H. Brokopf, D. Reinen, and O. Schmitz-Du Mont, Z. Phys. Chem. (Neue Folge) 68, 228 (1969).
[16]M. Tinkham, Proc. R. Soc. A 236, 535 (1956); 236, 549 (1956).
[17]J. W. Stout and R. G. Shulman, Phys. Rev. 118, 1136 (1960).
[18]M. T. Hutchings, B. D. Rainford, and H. J. Guggenheim, J. Phys. C 3, 307 (1970).
[19]J. Hubbard, D. E. Rimmer, and F. R. A. Hopgood, Proc. R. Soc. 88, 13 (1966).
[20]A. Trautwein, E. Kreber, U. Gonser, and F. E. Harris, J. Phys. Chem. Solids 36, 263 (1975); 36, 325 (1975).
[21]A. Trautwein, R. Zimmermann, and F. E. Harris, Theor. Chim. Acta 37, 89 (1975).
[22]R. Zimmermann, A. Trautwein, and F. E. Harris, Phys. Rev. B 12, 3902 (1975).
[23]A. Trautwein and F. E. Harris, Theor. Chim. Acta 30, 45 (1973).
[24]J. W. Stout and S. A. Reed, J. Am. Chem. Soc. 76, 5279 (1954).
[25]K. V. Krishna Rao, S. V. Nagender Naidu, and L. Lyengar, Current Sci. (India) 35, 280 (1966).
[26]A. Trautwein, F. E. Harris, A. J. Freeman, and J. P. Desclaux, Phys. Rev. B 11, 4101 (1975).
[27]R. Reschke and A. Trautwein, in Proceedings of the International Conference on the Application of the Mössbauer Effect, Corfu, Greece, Sept. 1976 (unpublished).
[28]H. M. Foley, R. M. Sternheimer, and D. Tycko, Phys. Rev. 93, 734 (1954).
[29]A. Trautwein, R. Reschke, I. Dézsi, and F. E. Harris, in Ref. 27.
[30]H. L. Schäfer and G. Gliemann, *Einführung in die Ligandenfeld-Theorie* (Akademische Verlagsanstalt, Frankfurt a.M. Germany, 1967).
[31]C. Kittel, *Introduction to Solid State Physics* (Wiley, New York, 1966), 3rd ed.
[32]Y. Jaccarino, in *Magnetism*, edited by G. T. Rado and H. Suhl (Academic, New York, 1965), Vol. 2, p. 307.
[33]R. C. Ohlmann and M. Tinkham, Phys. Rev. 123, 425 (1961).
[34]H. Wegener, *Der Mössbauer Effekt* (Bibliographisches Institut-Taschenbuch 2/2a, Mannheim, Germany, 1966).